LARGE EDDY SIMULATION OF TURBULENT SPRAY COMBUSTION IN AERONAUTICAL GAS TURBINES

S. Pascaud[1], M. Boileau[1], B. Cuenot[1] and T. Poinsot[2]

[1] *CERFACS, Toulouse, France*
[2] *IMFT, Toulouse, France*

Abstract   Reduction of pollutants emission or altitude re-ignition, strongly influenced by turbulent mixing and fuel spray evaporation, are critical issues for aeronautical gas turbine design. To understand unsteady spray combustion in industrial burners, Large Eddy Simulation (LES) is a unique and powerful tool. Its potential has been widely demonstrated for turbulent gaseous cold and reacting flows. Its extension to two-phase turbulent reacting flows is an obvious research path for the future. In the present work, an Euler-Euler formulation, together with a turbulent sub-grid scale model and a turbulent combustion model, is used to solve the conservation equations in each phase and the exchange source terms for mass, momentum and heat transfer. A stabilised turbulent spray flame in an aeronautical gas turbine is considered for application. Due to complex geometry, an unstructured mesh is used. The partially premixed flame structure revealed by LES is detailed. In particular, the role of evaporation and recirculation zones on the stabilisation mechanism is emphasized. Finally, LES and RANS results are compared.

Keywords   Large Eddy Simulation, spray, evaporation, combustion, complex geometry

CONTEXT

Large Eddy Simulations (LES) are rapidly becoming standard tools to study combustion in many modern combustion devices [1-6]. However, even though multiple proofs of the validity of the LES concept have been obtained for gaseous combustion, LES for two-phase flow combustion remains a much more difficult topic for which very few recent studies are available [7-10]. Considering that most fuels used for aeronautical applications are liquid, the need for two-phase combustion LES tools is obvious. The turbulent spray combustion involves several different physical phenomena such as particle dispersion, vaporisation, mixing and combustion. The dispersion is highly linked to the characteristics of the spray. Experimental studies on dispersion of solid particles [11] and vaporised droplets [12] have shown the influence of the Stokes number on the droplet trajectories. The isolated vaporising droplet model is a simple but useful description of the vaporising spray, required to understand the physics [13-17]. Different approaches have been used to analyse vaporising turbulent sprays : experiments [12, 18, 19], Direct Numerical Simulations (DNS) [20], LES [21] and Reynolds Averaged Navier Stokes (RANS) [18] or

turbulent spray combustion : experiments [22, 23], DNS [24-26], LES [27] and RANS [28, 29]. These recent studies exhibit the complexity of the multiple interactions between turbulence, two-phase flows and combustion. The aim of this paper is to use LES to analyse these unsteady correlations.

Modelling of the dispersed phase raises the question of the choice of the method used to couple the liquid and the gas phases in a LES formulation. In the Lagrange approach, the liquid phase is computed using a particle tracking method in which each droplet (or group of droplets) is computed individually giving its trajectory, velocity, temperature and diameter [7]. In the Euler approach, the liquid phase is homogeneized and solved for using a set of conservation equations for the liquid volume fraction, the liquid phase velocity and temperature, and the first/second order moments of the size distribution [30, 31]. The Lagrange framework is used in many applications because phenomena like droplet break-up, dispersion, interaction with walls and droplet/droplet interaction are easier to model. This choice may be revisited for the computation of unsteady spray combustion in complex geometry. The first argument comes from the numerics : LES are high CPU consumers; run on parallel computers. However, a significant amount of work is still needed to implement efficiently Lagrange algorithms on parallel computers [10]. Moreover, the cost of the Lagrange treatment increases rapidly with the number of droplets while the parallel efficiency decreases. On the other hand, Euler techniques are directly parallelised with the same algorithms than the gas phase computations. Another major issue for Lagrangian reacting two-phase LES is the number of droplets per cell required to provide a correct description of the liquid phase. LES being less dissipative than RANS, enough Lagrangian droplets must be used at each time step in each cell to provide a smooth and accurate continuous field of fuel mass fraction. Because the fuel vapour distribution, directly produced by the discrete droplet evaporation source terms, controls the propagation of the front [32, 33], this is crucial for two-phase flame computations. Very limited experience on this question is available today but it is likely that combustion requires much more particles than usually used for dispersion or evaporation studies, leading to uncontrolled CPU costs. Another advantage of Lagrange methods is that they naturally allow to track multisize droplet clouds. Size distribution controls the flame regime in many instances and must be taken into account. However, recent studies have demonstrated that Euler techniques may also be extended to include multisize liquid sprays [20, 34, 35]. Finally, a more general question regarding LES of two-phase flow combustion is the difficulty of specifying inlet conditions for the liquid phase: close to the fuel injectors, the droplet velocity and size distributions are not known with precision due to the complexity of primary atomization. The question then arises whether it is worth computing the dispersion of the fuel droplets with a high-precision

Lagrange method while using very approximate injection conditions. Close to the fuel injectors, the liquid phase is even not organized as droplets but more as liquid blobs [36] showing that the Lagrange method cannot even be used there. In these high-loading zones where no real drop exists, using the Euler approach may actually be more compatible with the physics of the liquid phase and the large uncertainties related to the fuel injection conditions.

In this paper, the Euler framework is chosen for LES. The parallel solver AVBP is described and the computation of a turbulent stable spray flame at atmospheric pressure in an industrial gas turbine sector is presented.

EQUATIONS

The Euler approach leads to similar conservation equations for both the carrier phase and the dispersed phase, on which LES filtering is then applied [37, 38]. For the carrier phase, the classical LES set of equations is recovered. It is coupled with the dispersed phase equations through phase exchange terms. The Favre averaged (defined as : $\tilde{\phi} = \frac{\overline{\rho\phi}}{\bar{\rho}}$) governing equations for gas and liquid mass and species conservation, momentum and total energy read :

$$\frac{D}{Dt}(\bar{\rho}) = \bar{\Gamma} \tag{1}$$

$$\frac{D}{Dt}(\bar{\rho}\tilde{Y}_k) = \frac{\partial}{\partial x_j}(\bar{\rho}\bar{D}_k\frac{\partial\tilde{Y}_k}{\partial x_j}) - \frac{\partial}{\partial x_j}(\bar{\rho}Y_{sgs}) + \bar{\dot{\omega}}_k + \bar{\Gamma}\delta_{kF} \tag{2}$$

$$\frac{D}{Dt}(\bar{\rho}\tilde{u}_i) = -\frac{\partial}{\partial x_i}\bar{p} + \frac{\partial}{\partial x_j}\bar{\tau}_{ij} - \frac{\partial}{\partial x_j}(\bar{\rho}u_{sgs}) + \bar{I}_i \tag{3}$$

$$\frac{D}{Dt}(\bar{\rho}\tilde{E}) = -\frac{\partial}{\partial x_j}\bar{q}_j + \frac{\partial}{\partial x_j}(\bar{\tau}_{ij}\tilde{u}_i) - \frac{\partial}{\partial x_j}(\bar{\rho}E_{sgs}) + \bar{\dot{\omega}}_T + \bar{I}_i\tilde{u}_i + \bar{\Pi} \tag{4}$$

$$\frac{D}{Dt}(\bar{\alpha}_l\bar{\rho}_l) = -\bar{\Gamma} \tag{5}$$

$$\frac{D}{Dt}(\bar{\alpha}_l\bar{\rho}_l\tilde{u}_{i,l}) = -\bar{I}_i \tag{6}$$

$$\frac{D}{Dt}(\bar{\alpha}_l\bar{\rho}_l\tilde{h}_{s,l}) = -\bar{\Pi} \tag{7}$$

$$\frac{D}{Dt}(\bar{n}) = 0 \tag{8}$$

In these equations, ρ (ρ_l) is the gas (liquid) mass density, Y_k is the mass fraction of the species k and u_i ($u_{i,l}$) is the gas (liquid) velocity. E is the total

non chemical energy of the carrier phase defined as : $E = e_s + \frac{1}{2}u_i u_i$ where e_s is the sensible energy and $h_{s,l}$ is the liquid sensible enthalpy. Finally, α_l is the volumic liquid fraction and n is the droplet density.

The stress tensor $\bar{\tau}_{ij}$ is assumed newtonian and the heat diffusion $\bar{q}_j$ is determined by the Fourier law. The unresolved turbulent fluxes $Y_{sgs} = \widetilde{u_j Y_k} - \tilde{V}^c_{k,j} \tilde{Y}_k$ and $E_{sgs} = \widetilde{u_j E} - \tilde{u}_j \tilde{E}$ are estimated by a classical gradient diffusion assumption. The subgrid stresses $u_{sgs} = \widetilde{u_i u_j} - \tilde{u}_i \tilde{u}_j$ are modeled with the WALE formulation [39].

The mass transfer Γ is expressed by the Spalding model [40] for spherical droplets :

$$\Gamma = \alpha_l \frac{6}{d^2} Sh(\rho D_\Gamma) ln(1 + B_M) \tag{9}$$

where the Sherwood Number Sh is equal to 2 and the Spalding number is defined by : $B_M = (Y_{F,\zeta} - Y_F)/(1 - Y_{F,\zeta})$ with ζ denoting the value at interface.

The momentum transfer is defined as $I_i = F_{d,i} + u_{i,l}\Gamma$ where $F_{d,i}$ is the standard drag force of a spherical droplet equal to $-\alpha_l \frac{3C_d}{4d} \rho_g |u_{i,l} - u_{i,g}|(u_{i,l} - u_{i,g})$. The drag coefficient C_d is, for $Re_d \geq 1000$, taken constant at 0.44 and equal to $\frac{24}{Re_d}(1 + 0.15\, Re_d^{0.687})$ otherwise, with the droplet Reynolds number defined as $Re_d = \frac{d}{v_g}|u_{i,l} - u_{i,g}|$.

The enthalpy exchange is :

$$\Pi = \Lambda + \Phi \tag{10}$$

where Λ is the contribution of mass transfer and Φ is the heat flux through the interface. The enthalpy transfer linked to evaporation is taken as $\Lambda = h_{F,\zeta}\Gamma$ where $h_{F,\zeta}$ is the sensible enthalpy of vaporised fuel. The heat flux is defined by $\Phi = \alpha_l \lambda Nu \frac{6}{d^2}(T_\zeta - T)$ where Nu is the Nusselt number and T_ζ is the temperature at the interface.

The reaction rate $\dot{\omega}_k$ and the heat release $\dot{\omega}_T$ are modeled by an Arrhenius law [41] with coefficients fitted by a genetic algorithm [42] from a reduced chemistry [43] to the present one-step chemistry : $JP10 + 14\, O_2 \rightleftharpoons 10\, CO_2 + 8\, H_2O$ using criteria such as flame speed and thickness. The fuel $JP10$ is a substitute for kerosene and has the same thermochemical properties. The flame/turbulence interaction is modeled by the thickened flame model [6].

THE LES CODE

The LES solver AVBP is a finite volume code, computing the equations for both phases with the same numerical method on the same unstructured mesh. It is explicit in time and takes into account the variations of molecular weights

and heat capacities with temperature and mixture composition. Boundary conditions used for inlets and outlet are non-reflective NSCBC conditions with relaxation coefficients [44]. Symmetry conditions are used on the burner sides, while non-slip adiabatic walls are used elsewhere. The unstructured mesh is composed of 2.3 million of tetrahedral elements. In this application, the time step is about $\Delta t = 0.2\mu s$. To calculate one turnover time of the swirled flow $\tau_{swirl} \simeq 3.5ms$, the LES computation of the turbulent spray flame takes one day on SGI ORIGIN 3800 on 64 processors.

CONFIGURATION

The configuration is a $1/16^{th}$ part of an annular combustion chamber. The geometry takes into account the main swirled inlet, the primary jets, the dilution jets and the cooling films that preserve the lower and upper walls from the flame. A sketch of the geometry and a view of the mesh are presented on Figure 1. The four primary jets are located on upper and lower walls, between the centered vertical plane and the sides of the burner, leading to highly turbulent impacts. Ten dilution jets are placed downstream to create a "cold wall" composed of cooling air, limiting the outlet temperature to preserve the downward turbine structure.

a.   b.
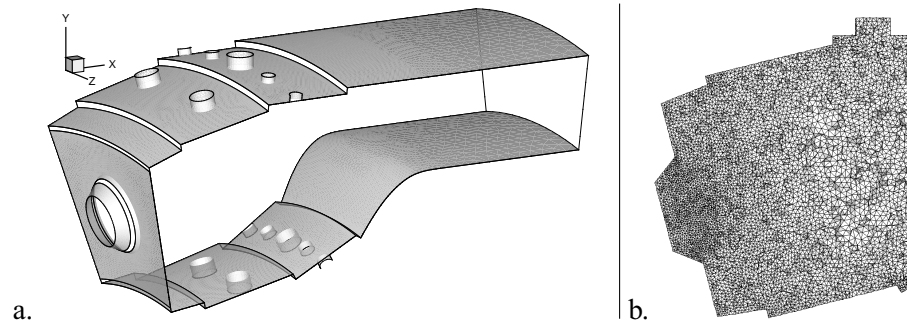
Figure 1: a. Geometry of the configuration, b. Mesh view (central plane)

INLET CONDITIONS

Air at 525 K is injected by two annular swirlers located upstream of the computational domain. The inner swirler is located between $r* = r/r_{max} = 0$ and 0.4, where r_{max} is the maximum radius of the outer swirler and $r*$ is defined as illustrated on Figure 2a. Using a cylindrical referential, the velocity components of the main swirled inlet (Figure 2b) are normalised by the bulk velocity U_{bulk} and noted with the symbol $*$. The normal and radial components

u_n^* and u_r^* are strongly influenced by both swirlers : their value is higher around the external radius of each swirler. The Reynolds number based on the bulk velocity U_{bulk} and the maximum injection radius r_{max} is equal to $Re = 15000$. The liquid fuel cone is defined by specifying $\alpha_l \simeq 10^{-3}$ in the inner zone and zero elsewhere, and taking the liquid velocity equal to the inlet gaseous velocity. The initial diameter of the kerosene droplets is $15\mu m$, and their temperature is $288\ K$. The Stokes number, based on the droplet relaxation time $\tau_p = \frac{\rho_l d^2}{18\mu} = 2.0\ ms$, is equal to $St = \frac{\tau_p}{\tau_{swirl}} \simeq 0.6$. This means that the droplet trajectories are quite correlated to the carrier phase motion. This correlation rises when the diameter of the vaporising droplets decreases.
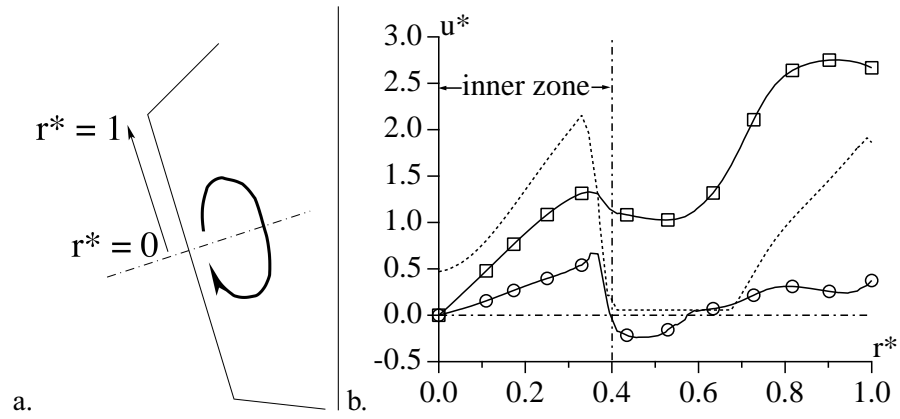
Figure 2: a. Definition of r*, b. Radial profiles of u_n^* ($\cdots$), u_r^* (—○—) and u_θ^* (—□—)

LES RESULTS

Dynamics

The swirled inlet generates a precessing motion and a recirculation zone, starting close to the fuel injection and stopped by the primary jets. The transversal half length of the recirculation zone is $r* \simeq 0.4 - 0.6$. An instantaneous view of the dynamics on the vertical central plane is presented on Figure 3a. The location of the primary jets, the dilution jets and the fuel injection is indicated. The solid line shows the zone where the axial velocity is opposite to the main flow direction. The impact of the primary jets on each other strongly influences the dynamics as illustrated on Figure 3b, where the y-component of the velocity is plotted on the plane of the primary jets.
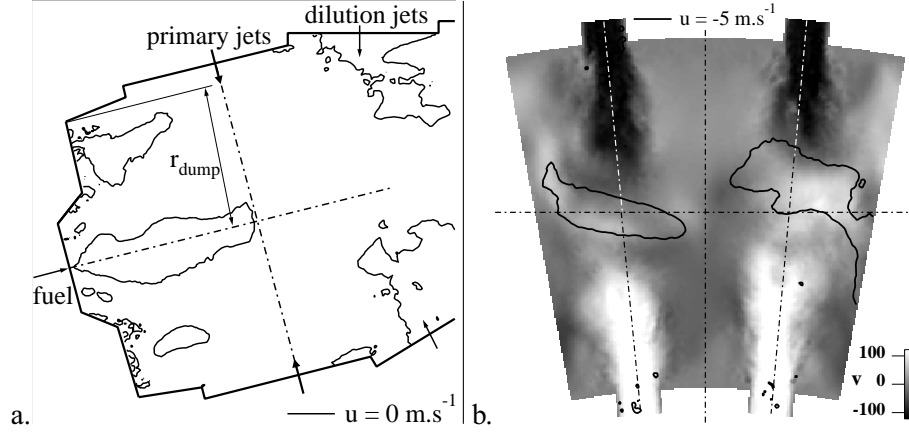
Figure 3: a. Back flow line, b. Primary jets : y-velocity field

Precessing Vortex Core

In its review on vortex breakdown [44], Lucca-Negro classifies the different topologies of swirling flows using the swirl number. One of these topologies at high swirl number is the precessing vortex core (PVC) : due to the swirl, the axial vortex breaks down at the stagnation point S and a spiral is created around a recirculation zone as illustrated on Figure 4a. In this application, the swirl number (based on r_{dump} defined on Figure 3a) is equal to :

$$S = \frac{1}{r_{dump}} \frac{\int_0^{r_{dump}} uwr^2\,dr}{\int_0^{r_{dump}} u^2 r\,dr} = 0.44 \tag{11}$$

Using the transverse plane A-B defined on Figure 5a, the backflow line is plotted on Figure 4b at six successive times marked with a number from 1 to 6 and separated by 0.5 *ms*. The precessing motion is then illustrated in the present configuration with a turnover time equal to $\tau_{swirl} \simeq 3.5ms$, corresponding to a frequency of $f_{PVC} \simeq 286\ Hz$.
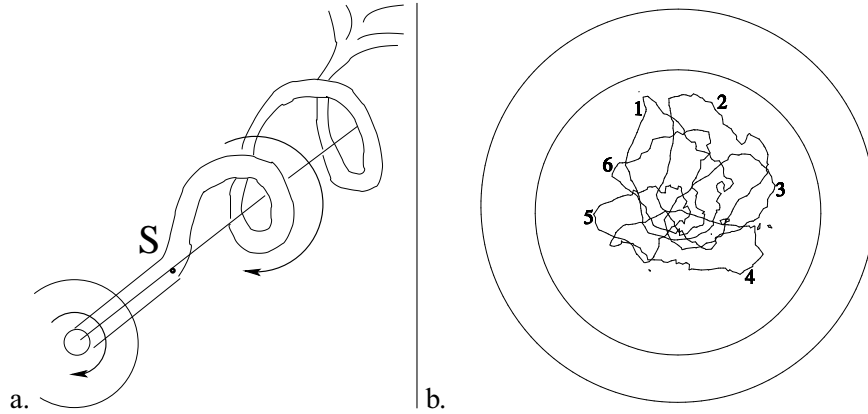
Figure 4: a. Sketch of the PVC ; b. Backflow line at six successive times

Dispersion

Due to their relatively low Stokes number, the droplets motion is controlled by the carrier phase so that the recirculation zone of the carrier phase and of the dispersed phase are similar. This can be observed on Figure 5a, where the $u = 0$ isolines of both phases are superposed. Since the droplets are constrained by the recirculation zone, they accumulate in a region close to the injector where the droplet density and the volumic fraction increase above the injection value. Radial dispersion by the swirl is also visible on Figure 5b.
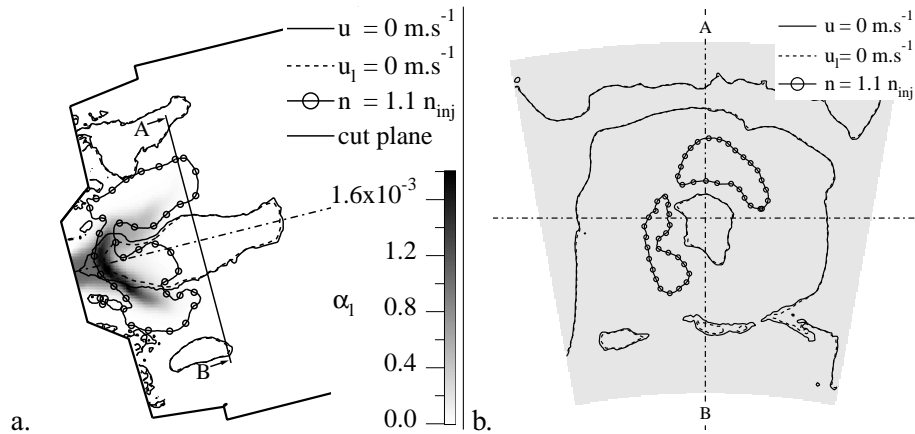
Figure 5: a. accumulation ; b. radial dispersion

Evaporation

Evaporation can be characterised on Figure 6 by the mass and heat transfer fluxes Γ and Π (see Equation 9 and Equation 10). The evaporation zone is located where fuel vapour is created. To describe the resulting fuel vapour distribution, the mixture fraction and local equivalence ratio are respectively defined by :

$$Z = \frac{sY_{JP10} - Y_{O_2} + Y_{O_2,0}}{sY_{JP10,0} + Y_{O_2,0}} \qquad (12)$$

$$\phi = \frac{Z}{1-Z} \frac{1-Z_{st}}{Z_{st}} \qquad (13)$$

with $Y_{O_2,0} = 0.233$, $Y_{JP10,0} = 1$ and $Z_{st} = 0.066$. In the evaporation zone, the mass transfer is high and leads to high variations of the local equivalence ratio. This zone is globally very rich as illustrated by the field of equivalence ratio on Figure 6a. The heat conduction Φ controlled by the temperature difference is relative and heats the droplets (reducing the air temperature as illustrated on Figure 6b) while the enthalpy transfer Λ linked to the mass transfer is positive. The global heat transfer Π takes positive values where the heat released by the flame front accelerates the evaporation.
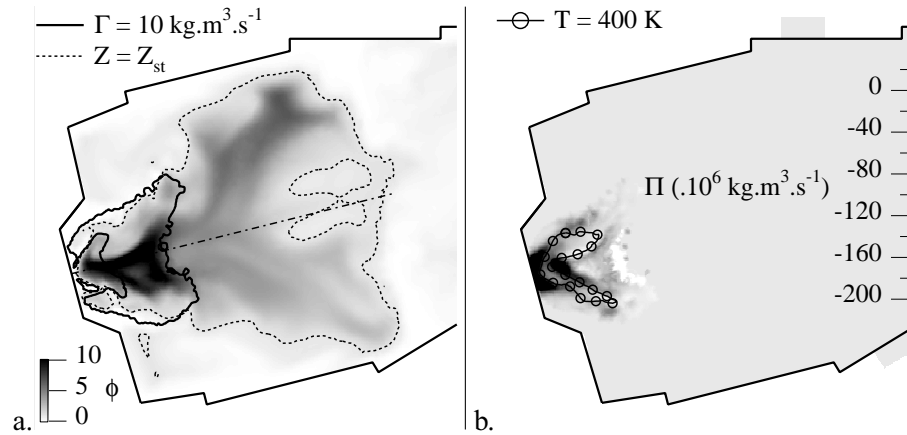
Figure 6: a. Equivalence ratio ϕ and mass transfer Γ, b. Heat transfer Π

Flame structure

The chemical reaction takes place where fuel vapour, oxidant and hot gases are simultaneously present. The evaporation zone brings fuel vapour and the

recirculation zone brings hot gases : the flame front, presented on Figure 7a, is attached to the evaporation zone and stabilised by the recirculation zone. It is actually composed of two successive fronts separated by the primary jets.

In order to distinguish premixed and diffusion flame fronts, the Takeno index $\mathcal{T} = \nabla Y_F . \nabla Y_O$ and an indexed reaction rate $\dot{\omega}_F^* = \dot{\omega}_F \frac{\mathcal{T}}{|\nabla Y_F|.|\nabla Y_O|}$ are used. The flame structure is then divided in two parts : $\dot{\omega}_F^* = +\dot{\omega}_F$ in premixed regime and $\dot{\omega}_F^* = -\dot{\omega}_F$ in diffusion regime. Results are shown on Figure 7b. Close to the dispersion and evaporation zones, the turbulent mixing between reactants create a rich partially premixed spray flame limited by the primary jets. By continuously creating pure fuel vapour, the evaporation process reinforces the partially premixed regime. An important point is that the reaction rate is very low there. The unburned fuel vapour and the cold air of the dilution jets then create a second flame front in the diffusion regime. This is clear through the Takeno index but also through the superposition of the reaction rate and the stoichiometric line.
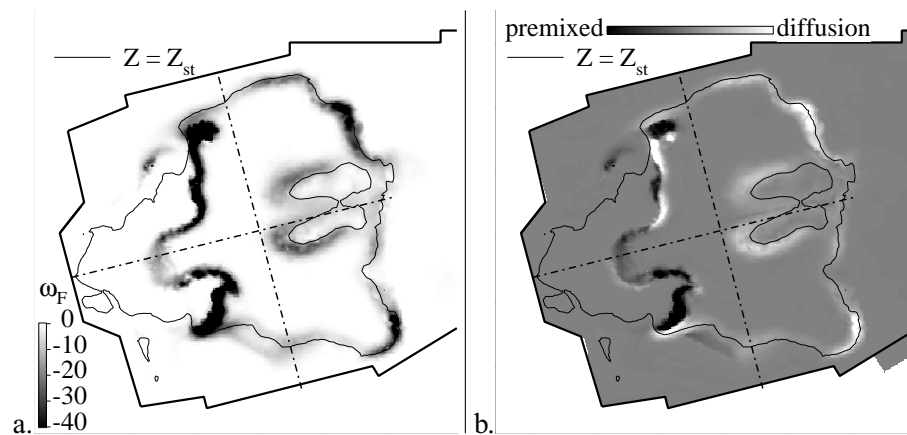
Figure 7: a. Reaction rate $\dot{\omega}_F$, b. Indexed reaction rate $\dot{\omega}_F^*$

Stabilisation mechanism

Classical combustion models of twin-fluid atomized jet spray [45, 46] are used to characterise the main competitive phenomena for flame stabilisation :

1. the air velocity must be low enough to match the turbulent flame velocity : the dynamics of the carrier phase (and in particular the main recirculation zone) stabilise the flame front on a stable pocket of hot gases

2. zones where the local mixture fraction is within flammability limits must exist : combustion occurs between the fuel vapour radially dispersed by

the swirl and the ambient air, where the equivalence ratio is low enough

3. the heat release must be high enough to maintain evaporation and reaction : the sum of heat flux Π and heat release $\dot{\omega}_T$, plotted on Figure 8a., allows to identify the zone (——) where the heat transfer due to evaporation extinguishes the flame : $\Pi + \dot{\omega}_T = 0$.

In the present case, the flame stabilisation is the result of mechanisms 1. and 3. : the flame starts in the recirculation zone where residence times are high enough, and is maintained at a certain distance by the cooling effect of evaporation. The mechanism 2. is not preponderant because the flow is within the flammability limit for a large range of the local mixture fraction, as illustrated by the mixture fraction diagram of reaction rate presented on Figure 8b.
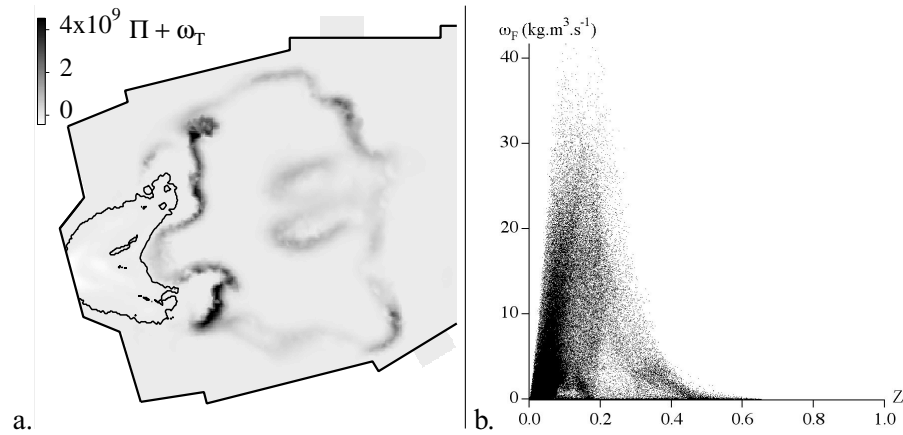
Figure 8: a. Sum of heat fluxes $\Pi + \dot{\omega}_T$; b. Reaction rate

PVC influence

The PVC generated by the swirl influences the dynamics of both the evaporation and combustion zones. The precessing unsteady evolution of fuel mass fraction (white solid line), heat release (black solid line) and temperature field is presented on Figure 9, on the transverse plane A-B defined on Figure 5a. The recirculation zones stabilise hot gases at the center of the combustion chamber and near the lateral sides. Between these hot regions, a cold annular zone corresponds to the evaporation domain. The fuel mass fraction isolines ($Y_{JP10} > 0.2$) are located in this zone and precess around the central recirculation zone. The flame motion is controlled by two main mechanisms : the central recirculation zone stabilises directly the flame front and evaporation brings fuel vapour to the flame. Therefore, the flame front also precesses around the central recirculation zone and is attached to the evaporation zone.

Time between each successive image : 0.5 ms ⇓
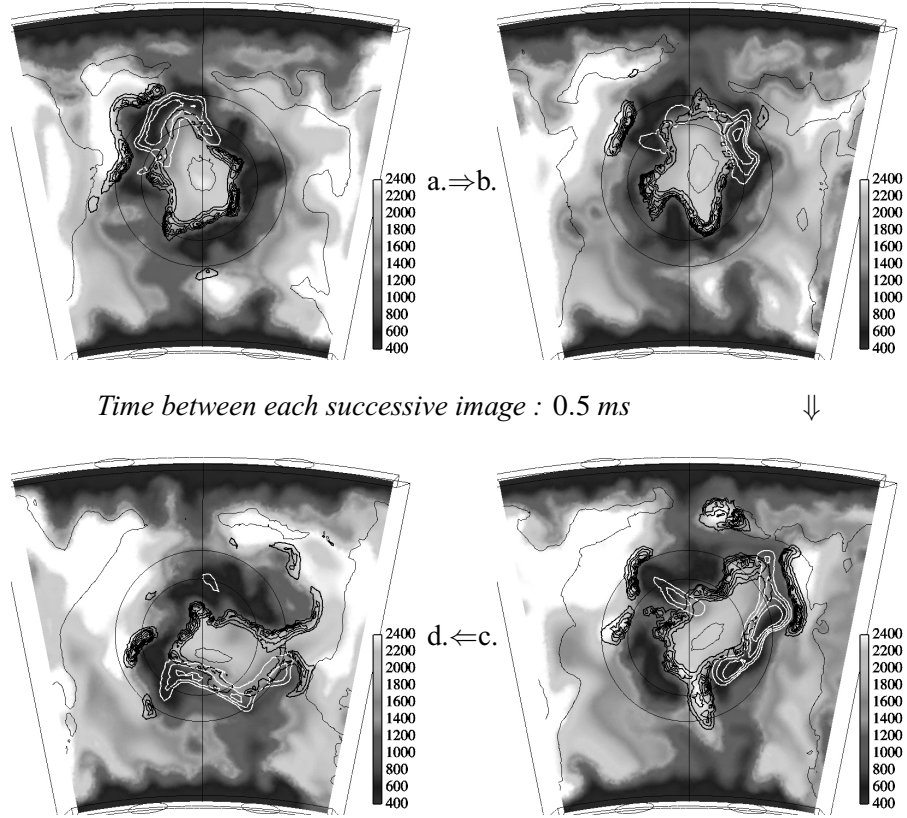
Figure 9: a.→d. Temperature field, fuel mass fraction (white solid line) and heat release (black solid line) at four successives times

AVERAGED FIELDS

Mixture fraction

Scatter plots of mean temperature T_g and oxygen mass fraction Y_{O_2} versus the mixture fraction are presented on Figure 10. Theoretical lines representing pure mixing ($- - -$) and infinitely fast chemistry ($—$) are also shown. Compared to gaseous combustion, the evaporation process implies main differences on the flame structure. First, the maximum mixture fraction does not exceed $Z_{max} = 0.65$ (with the reference fuel mass fraction fixed at $Y_{JP10,0} = 1$ in Equation 12). This corresponds to the maximum fuel mass fraction at the limit of saturation of the liquid fuel which is equal to $Y_{JP10,\zeta} = 0.65$. Second, in the evaporation zone, the gaseous temperature goes below the injection

temperature and therefore, below the mixing line. Third, for mixture fractions higher than the stoichiometric value (evaporation zone), the effects of mixing are stronger than the effects of chemistry because the high heat and mass transfers decrease the gaseous temperature and increase the local equivalence ratio. The structure of the obtained scatter plots can be analysed as in *Réveillon and al.*[25] studying the differences between gaseous and two-phase flames using a DNS approach. In particular, as presented on Figure 11, the intermediate lines corresponding to two-phase reaction can be identified.
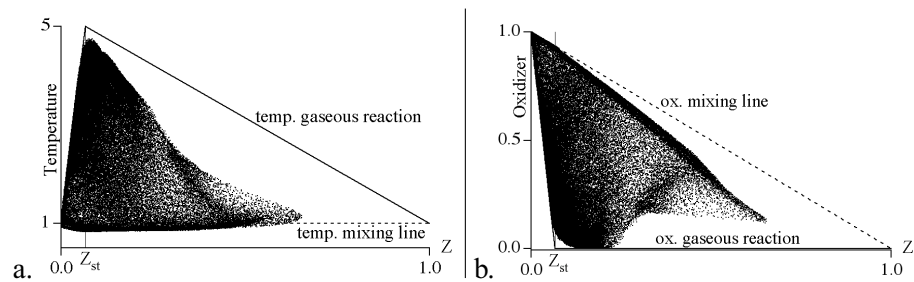
Figure 10: LES Mixture fraction diagrams
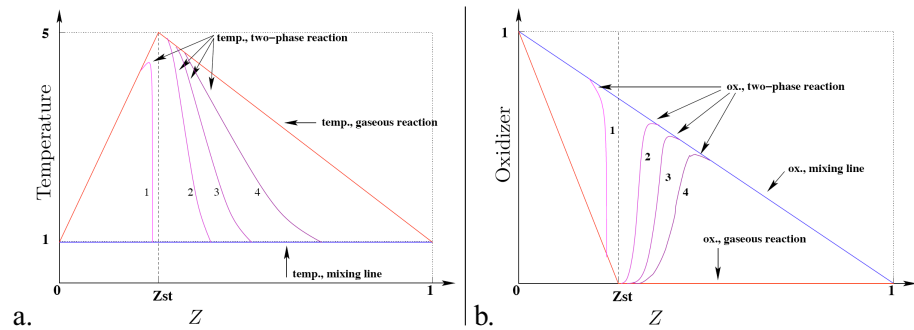
Figure 11: DNS Mixture fraction diagrams [25]

LES vs. RANS

For comparison, the same configuration has been run on the same mesh with the RANS code N3S using the models summarised in Table 1. Mean and fluctuating normalised velocities are compared on the vertical central plane at different cutting lines presented on Figure 12. The axial, radial and tangential components are respectively presented on Figure 13, Figure 14 and Figure 15. The main flow is strongly influenced by the jets penetration. The agreement

between LES and RANS is good on the mean velocities. However, LES leads to higher values of fluctuations. In the RANS approach, these fluctuations were simply approximated by $\frac{1}{3}k^{0.5}$. The fluctuating velocities are higher with the LES approach. Thanks to a higher turbulence level, the mean temperature field presented on Figure 16 is more rapidly homogenised in the LES case than in the RANS case. The influence of the dilution jets is higher in the RANS.

Table 1: AVBP and N3S models

Flow	*turbulent*	*spray*	*flame*
AVBP	LES (WALE)	Euler/Euler	Local thickening
N3S	RANS (k-ε)	Euler/Lagrange	Eddy Break-Up
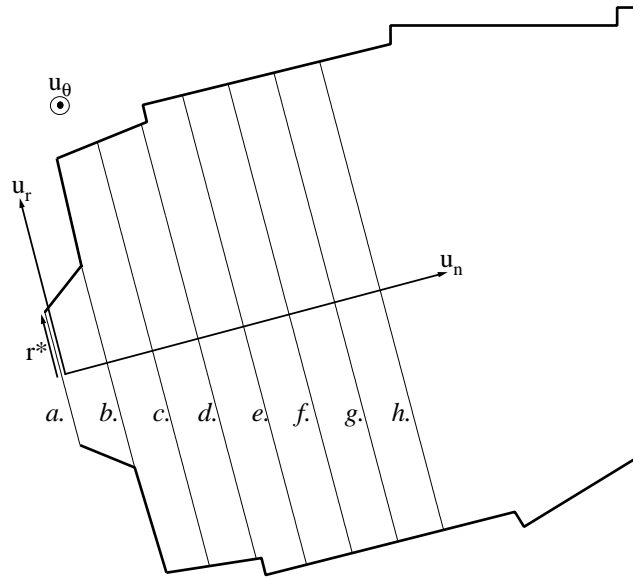
Figure 12: Sketch of cut lines
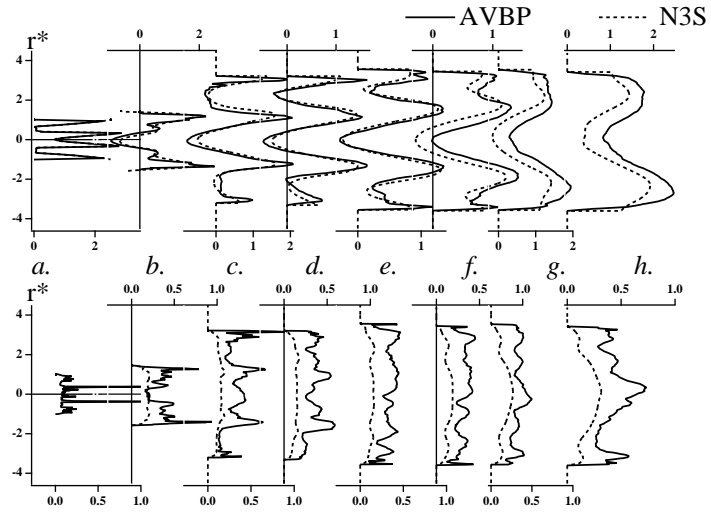
Figure 13: Axial velocity : $(u_n^*, u_n'^*)$
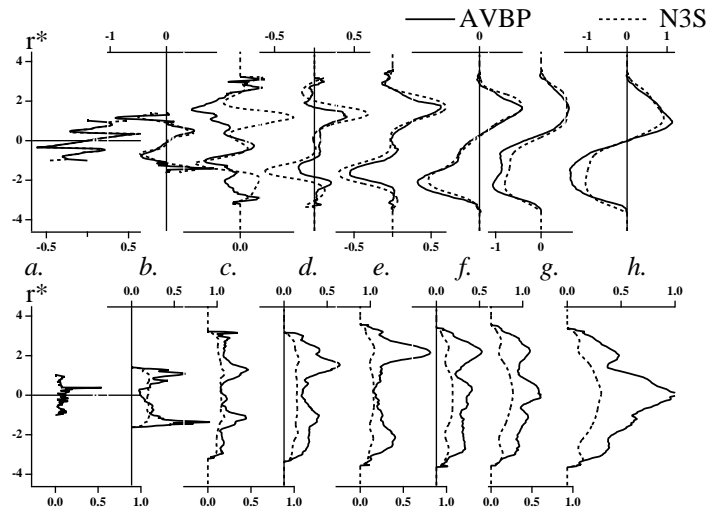
Figure 14: Radial velocity : $(u_r^*, u_r'^*)$
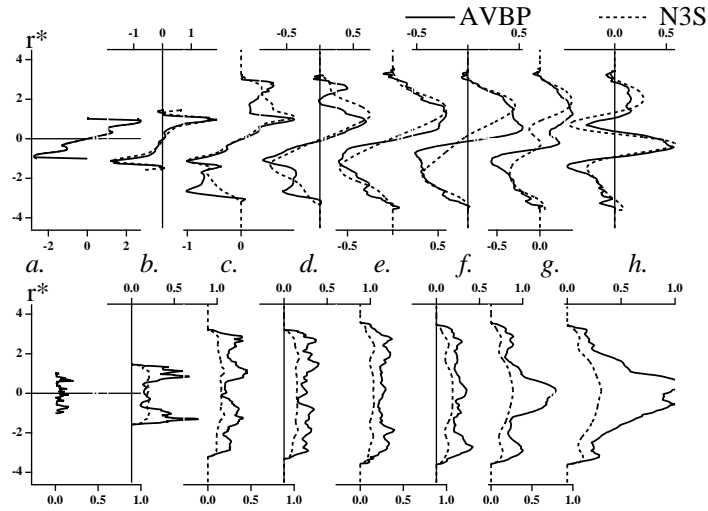
Figure 15: Tangential velocity : $(u_\theta^*, u_\theta'^*)$
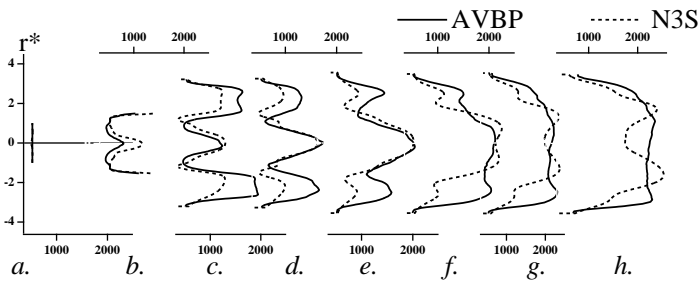
Figure 16: Mean temperature : T

CONCLUSION

The stabilised turbulent spray flame of an aeronautical gas turbine has been computed using the parallel LES code AVBP on an unstructured grid. Instantaneous and local results as well as steady mean results were both analysed and showed the good behaviour of the Euler model for the dispersed phase. The partially premixed flame structure was detailed and the importance of the evaporation on the flame topology was highlighted. The averaged results were quantitatively compared to the results of the RANS code N3S on the same configuration. Although the models used for turbulence, spray dispersion and combustion are different, mean fields proved to be very similar.

The LES approach brings here a totally new insight into the physics of such reactive two-phase flows, particularly on the unsteady mechanisms of a turbulent spray flame involving hydrodynamics (like the main swirled inlet and the transversal jets), particles dispersion and their evaporation, and combustion. The high variations of the local equivalence ratio in the evaporation zone and the stabilisation mechanism, controlled by both dynamics and evaporation are critical phenomena for such systems that deserve detailed and accurate studies. As a conclusion, this LES approach is a promising tool to investigate complex unsteady problems such as ignition, pollutant formation or response of a spray flame to complex acoustic perturbation.

REFERENCES

1. Desjardins P. E. and Frankel S. H. Two dimensional Large Eddy Simulation of soot formation in the near field of a strongly radiating nonpremixed acetylene-air jet flame. Combust. Flame; 119: 121-133, 1999.
2. Colin O., Ducros F., Veynante D. and Poinsot T. A thickened flame model for large eddy simulations of turbulent premixed combustion. Phys. Fluids; 12: 1843-1863, 2000.
3. Angelberger C., Egolfopoulos F. and Veynante D. Large Eddy Simulations of chemical and acoustic effects on combustion instabilities.Flow Turb. and Combustion; 65: 205-22, 2000.
4. Pitsch H. and Duchamp de la Geneste L. Large Eddy Simulation of Premixed Turbulent Combustion using a level-set approach.Proceedings of the Combustion Institute; 29: in press, 2002.
5. Pierce C. D. and Moin P. Progress-variable approach for large eddy simulation of non-premixed turbulent combustion. J. Fluid Mech.; 504: 73-97, 2004.
6. Selle L., Lartigue G., Poinsot T., Koch R., Schildmacher K.-U., Krebs W., Prade B., Kaufmann P. and Veynante D. Compressible Large-Eddy Simulation of turbulent combustion in complex geometry on unstructured meshes. Combust. Flame; 137: 489-505, 2004.
7. Mahesh K., Constantinescu G., Apte S., Iaccarino G., Ham F. and Moin P. Progress towards Large-eddy simulation of turbulent reacting and non-reacting flows in complex geometries. Annual Research Briefs; 115-142, 2002.
8. Mahesh K., Constantinescu G. and Moin P. A numerical method for Large-eddy simulation in complex geometries. J. Comput. Phys.; 197: 215-240, 2004.
9. Apte S. V., Gorokhovski M. and Moin P. Large-eddy simulation of atomizing spray with stochastic modeling of secondary breakup. ASME Turbo Expo 2003 - Power for Land, Sea and Air; 2003, Atlanta, Georgia, USA;
10. Ham F., Apte S. V., Iaccarino G., Wu X., Herrmann M., Constantinescu G., Mahesh K. and Moin P. Unstructured LES of reacting multiphase flows in realistic gas turbine combustors. Annual Research Briefs - Center for Turbulence Research; 2003.
11. Sommerfeld M. and Qiu H. H. Detailed measurements in a swirling particulate two-phase flow by a phase-Doppler anemometer.Int. J. Heat and Fluids Flows; 12: 1991.
12. Sommerfeld M. and Qiu H. H. Experimental studies of spray evaporation in turbulent flow.Int. J. Heat and Fluids Flows; 19: 10-22, 1997.

13. Gradinger T. B. and Boulouchos K. A zero-dimensional model for spray droplet vaporization at high pressures and temperatures.International Journal of Heat and Mass transfer; 2947-2959, 1998.

14. Miller R. S., Harstad K. and Bellan J. Evaluation of equilibrium and non-equilibrium evaporation models for many-droplet gas-liquid flow simulations.Int. J. Multiphase Flow; 1025-1055, 1998.

15. Catoire F., Gauthier J. E. D., Bardon M. F. and Benaissa A. Quasi-Steady-State Evaporation Model for Real Multi-component Fuel Droplets.Journal of the Institute of Energy; 134-142, 1999.

16. Réveillon J. and Vervisch L. Spray vaporization in nonpremixed turbulent combustion modeling : a single droplet model. Combust. Flame; 75-90, 2000.

17. Burger M., Schmehl R., Prommersberger P., Schaefer O., Koch R. and Wittig S. A multi-component droplet evaporation model for real aviation fuels at elevated pressures. ILASS-Europe; 2002, Zaragoza;

18. Gemci T., Hom J. and Chigier N. Simulation of evaporating spray and comparison with droplet temperature measurement obtained by rainbow refractometer. ASME Fluids Engineering Division; 2000,

19. Brandt M., Gugel K. O. and Hassa C. Experimental investigation of the liquid fuel evaporation in a premix duct for lean premixed and prevaporized combustion.J. of Eng. for Gas Turb. and Power; 119: 815-821, 1997.

20. Réveillon J., Massot M. and Pera C. Analysis and modeling of the dispersion of vaporizing polydispersed sprays in turbulent flows. Proceedings of the Summer Program 2002 - Center for Turbulence Research; 2002,

21. Caraeni D., Bergström C. and Fuchs L. Modeling of liquid fuel injection, evaporation and mixing in a gas turbine burner using Large Eddy Simulations.Flow Turb. and Combustion; 223-244, 2000.

22. Presser C., Gupta A. K. and Semerjian H. G. Aerodynamic characteristics of swirling spray flames : pressure-jet atomizer. Combust. Flame; 25-44, 1993.

23. Sornek R. J., Dobashi R. and Hirano T. Effect of turbulence on vaporization, mixing, and combustion of liquid-fuel sprays. Combust. Flame; 120-479, 2000.

24. Sirignano W. A. Theoretical Foundations for the Analysis of Laminar and Turbulent Spray Flows. Proceedings of the Western States Section/Combustion Institute Fall Meeting; 2003,

25. Réveillon J. and Vervisch L. Analysis of weakly turbulent diluted-spray flames and spray combustion diagram.Under consideration for publication in J. Fluid Mech.; 2004.

26. Vervisch L., Hauguel R., Domingo P. and Rullaud M. Three facets of turbulent combustion modelling: DNS of premixed V-flame, LES of lifted nonpremixed flame and RANS of jet flame.J. of Turb.; 5: 004, 2004.

27. Sankaran V. and Menon S. LES of spray combustion in swirling flows.J. of Turb.; 3: 011, 2002.

28. Klose G., Schmehl R., Meier R., Meier G., Koch R., Wittig S., Hettel M., Leuckel W. and Zarzalis N. Evaluation of advanced two-phase flow and combustion models for predicting low emission combustors. ASME Turbo Expo 2000. 45th ASME Gas Turbine and Aeroengine Congress; 2000, Munich;

29. Guo Y. C., Chan C. K. and Lau K. S. A pure Eulerian model for simulating dilute spray combustion.Fuel; 2131-2144, 2002.

30. Pandya R. and Mashayek F. Two-fluid large-eddy simulation approach for particle-laden turbulent flows.Int. J. Heat and Mass Transfer; 45: 4753-4759, 2002.

31. Riber E., Moreau M., Simonin O. and Cuenot B. Towards Large Eddy Simulation of Non-Homogeneous Particle Laden Turbulent Gas Flows Using Euler-Euler Approach. 11th Workshop on Two-Phase Flow Predictions; 2005, Merseburg, Germany;

32. Pitsch H. and Peters N. A consistent flamelet formulation for non-premixed combustion considering differential diffusion effects. Combust. Flame; 114: 26-40, 1998.

33. Selle L., Lartigue G., Poinsot T., Kaufman P., Krebs W. and Veynante D. Large Eddy Simulation of turbulent combustion for gas turbines with reduced chemistry. Proceedings of the Summer Program - Center for Turbulence Research; 2002, 333-344

34. Borghi R. Background on droplets and sprays. Combustion and turbulence in two phase flows, Lecture Series 1996-02; 1996,

35. Delabroy O., Lacas F., Labegorre B. and Samaniego J.-M. Paramètres de similitude pour la combustion diphasique.Rev. Gén. Therm.; 934-953, 1998.

36. Reitz R. D. and Diwakar R. Structure of high pressure fuel sprays. Tech. Rep. 870598. SAE Technical Paper. 1987

37. Simonin O. Continuum modelling of dispersed two-phase flows. Combustion and turbulence in two phase flows, VKI Lecture Series 1996-02; 1996, Von Karman Institute for Fluid Dynamics;

38. Février P., Simonin O. and Squires K. Partitioning of particle velocities in gas-solid turbulent flows into a continuous field and a spatially-uncorrelated random distribution : theoretical formalism and numerical study.submitted to J. of Fluid Mech.; 2005.

39. Nicoud F. and Ducros F. Subgrid-scale stress modelling based on the square of the velocity gradient.Flow Turb. and Combustion; 62: 183-200, 1999.

40. Spalding D. B. The combustion of liquid fuels. 4th Symposium (Int.) on Combustion; 1953, Combustion Institute, Baltimore, MD; 847-864

41. Poinsot T. and Veynante D. Theoretical and numerical combustion, 2001.

42. Martin C. EPORCK User Guide V1.8. 2004

43. Li S. C., Varatharajan B. and Williams F. A. The chemistry of JP-10 ignition.AIAA; 39: 2351-2356, 2001.

44. Poinsot T. and Lele S. Boundary conditions for direct simulations of compressible viscous flows. J. Comput. Phys.; 101: 104-129, 1992.

45. Gupta A. K., Lilley D. G. and Syred N. Swirl flows, 1984.

46. Chigier N. A. Application of model results to design of industrial flames. Proc. of 4th symposium of flames and industry; 1972, IC, London;

ACKNOWLEDGEMENTS